Turbulence Spectra and Dissipation Rates in a Wind Tunnel Model of the Atmospheric Convective Boundary Layer

ROLF KAISER AND EVGENI FEDOROVICH

Institut für Hydrologie und Wasserwirtschaft, Universität Karlsruhe, Karlsruhe, Germany

(Manuscript received 13 May 1996, in final form 17 June 1997)

ABSTRACT

A model of the atmospheric convective boundary layer (CBL) is realized in the thermally stratified wind tunnel of the Institute of Hydrology and Water Resources, University of Karlsruhe. Further experimental results from this model are presented. The wind tunnel with a test section 10 m long, 1.5 m wide, and 1.5 m high allows one to generate a quasi-stationary, horizontally evolving CBL, characterized by convective Richardson numbers $\mathrm{Ri}_{\Delta T}$ up to 10 and Ri_N up to 20, with the bottom shear/buoyancy dynamic ratio u_*/w_* in the range of 0.2 to 0.5. The convective regime in the tunnel is dominated by bottom-up forcings. Effects of entrainment in the simulated CBL play a secondary role.

The spectra of turbulence in the wind tunnel flow are calculated from high-resolution velocity component and temperature time series, simultaneously measured using laser Doppler and resistance-wire technique, respectively. The spectra from the mixed core of the CBL and in the entrainment zone display pronounced inertial subranges. The ratio of vertical to horizontal velocity spectra in these subranges is within the interval from 1.3 to 2, which is slightly larger than could be expected for purely isotropic turbulence. Different maxima in the production ranges of the spectra are related to dominant turbulence scales in the wind tunnel flow. The energy-containing ranges of the wind tunnel spectra exhibit plateaulike shapes resulting from modification of the turbulence production by the flow shear. The comparison with atmospheric spectra and spectral data from water tank and large eddy simulation studies of the CBL suggests that the turbulence spectral regime in the tunnel flow has much in common with its atmospheric prototype.

The turbulence kinetic energy dissipation rate and the destruction rate of temperature fluctuations are evaluated based on the relationships resulting from the Kolmogorov theory for the inertial-subrange spectra. The dissipation rates obtained are within the scatter ranges of data from atmospheric measurements and model studies of convection. High dissipation values in the lower portion of the simulated CBL are indicative of the shear enhancement of turbulence production in the wind tunnel convective flow.

1. Introduction

Motions of a variety of scales constitute the turbulent flow in the atmospheric convective boundary layer (CBL). In the absence of mean wind, which is the case of a shear-free CBL, turbulence is solely maintained by buoyant forcing. This forcing favors vertical motions and leads to the characteristic cellular convection pattern composed of thermals (warm updrafts) and associated cool downdrafts. Although buoyancy is the dominant forcing mechanism in the CBL, wind shear at the surface can substantially modify the CBL flow structure. With an increasing shear contribution, the cellular flow pattern is replaced by a composition of roll-like motions. This transition between the two turbulence regimes could be observed most clearly in the vertical velocity patterns from the large eddy simulations (LES) of convection (Sykes and Henn 1989; Mason 1992; Moeng and Sullivan 1994).

Under conditions (or assumptions) of statistical homogeneity on large horizontal scales, the CBL temporal evolution may be regarded as a nonstationary process. Most numerical and laboratory model studies carried out so far dealt with this nonstationary CBL. Available measurement data on the convective turbulence structure in the atmosphere also refer to such a CBL case. Another case of the CBL is the horizontally evolving one, which grows by advection-type entrainment in a quasi-stationary, neutrally or stably stratified air flow over the heated underlying surface. This type of CBL can be reproduced in a wind tunnel. We are not aware of any laboratory experiments on modeling the horizontally evolving CBL in either water tanks or water channels. In the atmosphere, especially with mean wind and over nonuniform terrain, the CBL flow pattern varies both in time and space. The comparison of turbulence statistics, evaluated from the wind tunnel measurements by temporal averaging, with spatial averages from water tank and LES studies (Fedorovich et al.

Corresponding author address: Dr. Evgeni Fedorovich, Institut für Hydrologie und Wasserwirtschaft, Universität Karlsruhe, Kaiserstraße 12, 76128 Karlsruhe, Germany.
E-mail: evgeni.fedorovich@bau-verm.uni-karlsruhe.de

1996, hereafter referred to as FKRP) suggests that turbulence regimes in the nonstationary CBL and in the horizontally evolving CBL are quite similar.

In the present paper we show further model results from the thermally stratified tunnel described in Poreh et al. (1991) and Rau and Plate (1995). The design of the tunnel, which has a 10 m × 1.5 m × 1.5 m test section, allows preshaping the velocity and temperature profiles at the inlet of the test section. This provides the opportunity to generate a developed CBL over comparatively short fetches.

For presenting spectral data in dimensionless form we shall use the traditional Deardorff (1970) convective scales for length, velocity, and temperature, which respectively are

$$z_i, \qquad w_* = (\beta Q_s z_i)^{1/3}, \qquad T_* = Q_s/w_*, \qquad (1)$$

where z_i is the CBL depth, usually defined as the altitude of the most negative flux of entrainment at the CBL top, Q_s is the turbulent kinematic heat flux at the surface, and β is the buoyancy parameter. The procedure for the determination of the Deardorff (1970) scales from velocity and temperature profiles measured in the wind tunnel is described in FKRP.

The convective flow in the wind tunnel is characterized by moderate values of Richardson numbers $\mathrm{Ri}_{\Delta T} = \beta w_*^{-2} z_i \Delta T$ (<10), representing the effect of the temperature increment ΔT across the capping inversion, and $\mathrm{Ri}_N = N^2 z_i^2 w_*^{-2}$ (<20), representing the damping effect of the stable stratification above the CBL, with N as the buoyancy frequency. These Ri values indicate that the convective regime in the tunnel corresponds to such conditions in the atmosphere, when both capping inversion and hydrostatic stability of the upper air are not very strong. Experimental results given in FKRP show that the turbulence regime in the simulated CBL is mainly determined by bottom-up forcings, which are convective heat transfer and shear at the underlying surface. The entrainment and associated negative turbulent heat flux across the entrainment zone are weak. Moderate inversion strength leads to smaller temperature fluctuations in the upper part of the CBL as compared with data from studies with larger $\mathrm{Ri}_{\Delta T}$, and monotonic decay of the horizontal velocity variance within the entrainment layer. The bottom-up buoyancy/shear ratio u_*/w_* in the range from 0.2 to 0.5, where u_* is the friction velocity, results in a noticeable increase of velocity component variances in the lower portion of the layer compared with the shear-free CBL.

Cells in the shear-free CBL and rolls in the sheared CBL represent large-scale components of turbulent motion, which are quasi-steady and semiorganized. Such large eddy coherent structures usually contain most of the energy in the CBL turbulence spectra. Analyzing vertical velocity spectra (hereafter *w* spectra) measured in the atmospheric CBL, Grossman (1982) concluded that persistent peaks and dips in these spectra at low wavenumbers are caused by coherent structures. Nevertheless, most atmospheric studies of the CBL turbulence spectra, for instance those of Kaimal et al. (1976), Caughey and Palmer (1979), Young (1987), and Mann et al. (1995), give no evidence of resolved spectral structures indicating the separation of scales in the CBL organized motions. Usually, spectra measured in the bulk of the atmospheric CBL merely reveal a peak of energy at scales of the order of the CBL depth. This feature of the atmospheric spectra is easy to explain by a multitude of disturbing nonconvective forcings affecting the flow pattern in the atmospheric CBL (Sorbjan 1991). In the *w* spectra from the LES of the shear-free CBL, Schmidt and Schumann (1989) found distinctive peaks at wavelengths corresponding to the horizontal scales of updrafts and downdrafts. Deardorff and Willis (1985) observed similar peaks in spectra from their water tank model of the shear-free CBL. They nevertheless did not consider them as statistically significant due to data randomness and finite sampling.

Smaller-scale turbulent fluctuations in the CBL do not show consistent features of organization. One can expect, however, that their magnitude may be affected by larger semiorganized motions as a result of the energy cascade from larger eddies to smaller ones. From the LES model of the shear-free CBL, Schmidt and Schumann (1989) reported the persistent domination of vertical motions over the horizontal ones at comparatively large wavenumbers, where the effect of pressure fluctuations was still not strong enough to create locally isotropic turbulence. Nevertheless, the velocity spectra values from this study approximately agreed with the predictions of the inertial-subrange theory, which assumes that within the inertial energy cascade the spectral density depends only upon the wavelength and the turbulence kinetic energy (TKE) dissipation rate. In the Deardorff and Willis (1985) water tank model of the shear-free CBL, the inertial subranges in the velocity spectra were quite short and might be observed only in spectra referring to the lower half of the water tank CBL. The ratio of *w* spectra to horizontal velocity spectra (hereafter *u* spectra) in the Deardorff and Willis (1985) experiments was closer to the theoretical value of 4/3 for isotropic turbulence.

The atmospheric CBL velocity spectra usually display extended inertial subranges at large wavenumbers. Kaimal et al. (1976) from tethered balloon and Young (1987) from aircraft measurements found that in the inertial subrange the employment of Deardorff (1970) convective scales together with the TKE dissipation rate as controlling parameters allows one to project the CBL spectra onto one curve. Young also tested the above scales for normalizing the temperature spectra (hereafter *T* spectra), with the temperature fluctuation destruction rate used as one more controlling parameter. He came to the conclusion that the normalization of temperature spectra by convective scaling works within a shorter range of wavenumbers compared to the vertical velocity spectra. The normalized *T* spectra, in contrast to the *w*

spectra, retain a marked dependence on the dimensionless height z/z_i. Besides the effect of entrainment, which modifies the atmospheric temperature spectra in the upper portion of the CBL, they are additionally affected by the mesoscale variability of the temperature field, which mainly contributes to the longwave spectrum components. Both forcings are not accounted for by the Deardorff (1970) convective scaling. There is no clear indication in the experimental and model data published regarding the modification of the temperature variance in the CBL by wind shear.

While the spectral structure of turbulence in the shear-free CBL was comprehensively studied during the last several decades, both experimentally and with numerical models, the spectral characteristics of turbulence in the sheared CBL are much less investigated. In the spectra from atmospheric measurements, especially in those of the horizontal velocity components, and at longer wavelengths, the contribution of shear cannot be appropriately determined due to the contamination of the velocity field by mesoscale motions. When discussing the well-known problem of discrepancies between LES and atmospheric data on the horizontal velocity variance in the CBL (Schmidt and Schumann 1989; Nieuwstadt et al. 1993), the effects of shear and mesoscale variability in the atmosphere are often mentioned together as a combined source of these discrepancies. We know of no LES study published that focuses on the spectral analysis of turbulence in the CBL with shear. If such a study is done once [as can be concluded from Moeng and Sullivan (1994) it is just a matter of time], the problem of experimental verification of the LES predictions will arise. Water tank models of the atmospheric CBL can hardly be considered promising with this respect. Traditionally, and due to certain technical problems, they deal only with the shear-free convection (Deardorff and Willis 1985; Adrian et al. 1986; Kumar and Adrian 1986; Cenedese and Querzoli 1994).

Spectral data presented below refer to the CBL cases previously considered in FKRP. The spectra have been derived from the same time series as used in FKRP for evaluating mean-flow parameters and turbulence statistics in the horizontally evolving sheared CBL. The employed procedure of spectra calculation will be described in section 2 and in the appendix. Velocity, temperature, and heat flux spectra at different fetches along the test section of the tunnel and at different altitudes within and above the simulated CBL will be discussed in section 3. The comparison of the wind tunnel spectra with the CBL spectral data from atmospheric measurements, water tank, and LES studies will be presented in this section as well. The TKE dissipation rate and the destruction rate of temperature fluctuations in the wind tunnel model of the CBL will be analyzed in section 4 together with data from other CBL studies. Concluding remarks are adduced in section 5.

2. Spectra derivation from measured time series

For measuring vertical and horizontal flow velocity components in the wind tunnel a two-component laser Doppler velocimetry (LDV) system is used. Details of the measuring procedure are given in FKRP. To obtain velocity time series, the LDV processor is operated in the even-time coincidence mode. In each even-time window only the first velocity signal is registered. The width of the even-time window is 0.01 s, which provides a sampling frequency of 100 Hz. The typical data rate value (number of particles crossing the control volume per second) in the bulk of the CBL is within the range from 300 to 1500 Hz depending on the measurement altitude. With a data rate being from 3 to 15 times higher than the sampling frequency, the velocity field is sampled quasi-equidistantly in time. Each time series consists of 16 384 values.

The temperature in the wind tunnel flow is measured by a 2.5-μm resistance wire with a cutoff frequency of 300 Hz. Discretization of the analog signal of the resistance wire is triggered by the LDV signal in order to synchronize the velocity and temperature time series. The temperature probe is placed at the same level as the LDV measuring volume, and shifted 1 mm downstream. This shift desynchronizes velocity and temperature measurements at frequencies of 1000 Hz and more (the mean-flow velocity in the tunnel is 1 m s^{-1}). As will be seen from the spectra shown below, at these frequencies the energy of both velocity and temperature turbulent fluctuations is small compared with the energy in the resolved frequency range. Thus, the velocity and temperature measurements in the tunnel can be regarded as coincidental in time and space.

We calculate spectral densities by the finite Fourier transforms of the original time series based on the Wiener–Khinchin relationship. This relationship equates the spectral densities to the one-sided spectral density functions defined in terms of Fourier transforms of correlation functions (Bendat and Piersol 1986; see appendix). Since the introduction of algorithms for fast Fourier transforms by Cooley and Tukey (1965), this approach toward the discrete spectra calculation has become dominant.

3. Velocity, temperature, and heat flux spectra

a. Velocity spectra

Spectral data considered hereafter represent the basic flow configuration from FKRP. We shall begin by discussing the vertical and horizontal variability of the velocity spectra in the wind tunnel CBL.

Figure 1 illustrates the *w*-spectrum evolution within the CBL entrainment zone. In the case under consideration, this zone is located roughly between $0.8z/z_i$ and $1.2z/z_i$. All spectra shown refer to the first measurement location within the developed CBL (see FKRP), that is to $x = 3.98$ m. The largest spectral values in the plot

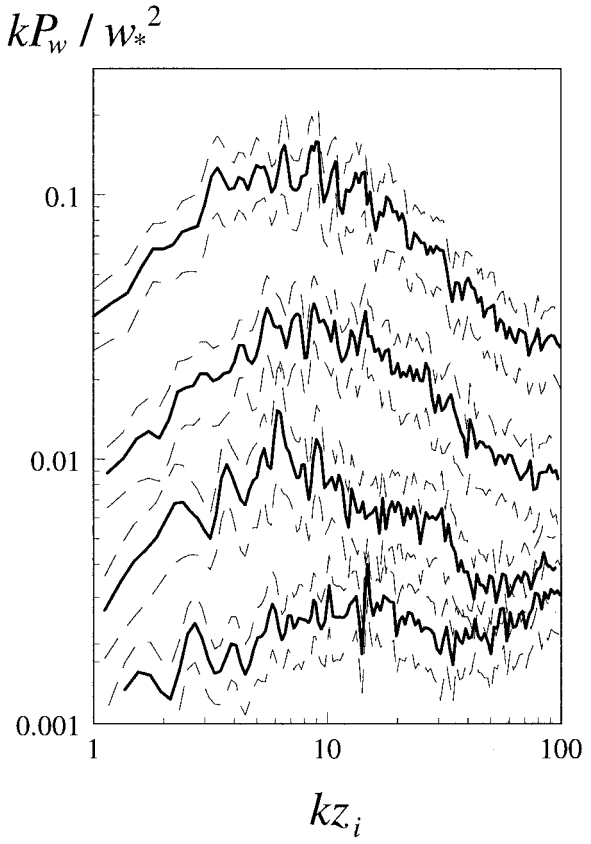

FIG. 1. Changes of the vertical velocity spectrum with height in the upper portion of the simulated CBL, at $x = 3.98$ m. The dashed lines represent 90% confidence limits. The spectra correspond to $z/z_i = 0.75$ (the uppermost spectrum), $z/z_i = 1$, $z/z_i = 1.2$, and $z/z_i = 1.4$ (the lowest spectrum).

are observed slightly beneath the entrainment region, at $z/z_i = 0.75$, where the turbulence regime is still mainly governed by bottom-up buoyancy forcing and subordinate shear forcing. The overall shape of the spectrum near its maximum is quite flat. However, several local peaks can be identified in the spectrum at a number of wavelengths. The two highest peaks, roughly of equal magnitude, refer to $kz_i = 6$ and $kz_i = 9$, thus corresponding approximately to the wavelengths of z_i and $0.7z_i$. These peaks are apparently associated with typical length scales of the vertical velocity perturbations produced by updrafts (thermals) and downdrafts passing the measurement volume. The characteristic size of large-scale convective structures revealed by flow visualizations in FKRP is approximately within the above-scale range. In the midst of the entrainment layer, at $z/z_i = 1$, the energy of the w fluctuations drops, and the spectrum in the vicinity of its maximum, which is located close to $kz_i = 9$, gets relatively narrow, thus indicating a narrower range of representative turbulence scales. The comparison of the entrainment layer spectrum with the spectrum measured at $z/z_i = 0.75$ certifies that this reduction of production range length takes place mainly at the expense of the lower frequency perturbations. Local peaks placed around the spectrum maximum are still persistent in the entrainment layer spectrum. Higher on, at $z/z_i = 1.2$, the energy of the w fluctuations reduces to values of an order of magnitude smaller than at the lower interface of the entrainment zone. The corresponding spectrum is characterized by two distinct peaks at the wavelengths close to the positions of peaks pointed out in the first spectrum—namely, at $kz_i = 6$ and $kz_i = 9$. Flow visualization patterns and temperature skewness profiles from FKRP suggest that the horizontal dimensions of the thermals in this range of heights are of the same order as in the flow region below the entrainment zone. However, the separation distances between the thermals are typically larger in the vicinity of the CBL top.

Above the entrainment layer, in the stably stratified flow ($z/z_i = 1.4$), the high-wavenumber spectrum is noticeably contaminated by both spectral aliasing and high-frequency noise. Their combined effect is seen in the right-hand field of the plot as a rising of the spectral curve. The influence of noise on the spectra essentially depends on the signal-to-noise ratio, which is relatively small above the CBL. Main sources of noise in the measured spectra are digitization of the analog laser Doppler burst signal (due to the finite temporal resolution of the analog to digital converter there is an estimated error of about 0.4% in the determination of the Doppler frequency) and nonequidistant sampling of the time series, which mainly affects the high-frequency spectral range.

Examples of u and w spectra at different fetches corresponding to the progressive CBL growth, and at three dimensionless elevations above the test-section floor are given in Fig. 2. Generally, the normalized spectra of both components at a given z/z_i retain their shapes during the process of the CBL development. This is an indication for the approximate self-similarity of the turbulence spectral regime in the simulated CBL. The shear contribution in the lower and middle portions of the layer enhances the energy of the velocity fluctuations. The role of shear in the enhancement of the velocity component variances at early stages of the CBL evolution, in particular at $x = 3.98$ m, was discussed in FKRP. As seen from the spectra plotted, such enhancement is more pronounced at larger wavenumbers ($kz_i > 7$).

This suggests that, in the bulk of the CBL, the buoyancy acts as the dominant factor of turbulence production at smaller wavenumbers, while the contribution of shear becomes important with increasing wavenumbers. However, the scaling applied to the measured spectra takes into account solely the buoyancy contribution. The joint effect of buoyant and shear forcings leads to an elongation of the production range and to the relative flatness of the normalized spectra in the high-wavenumber portion of this range. Both of these features are clearly seen in the w spectra and to a smaller extent in

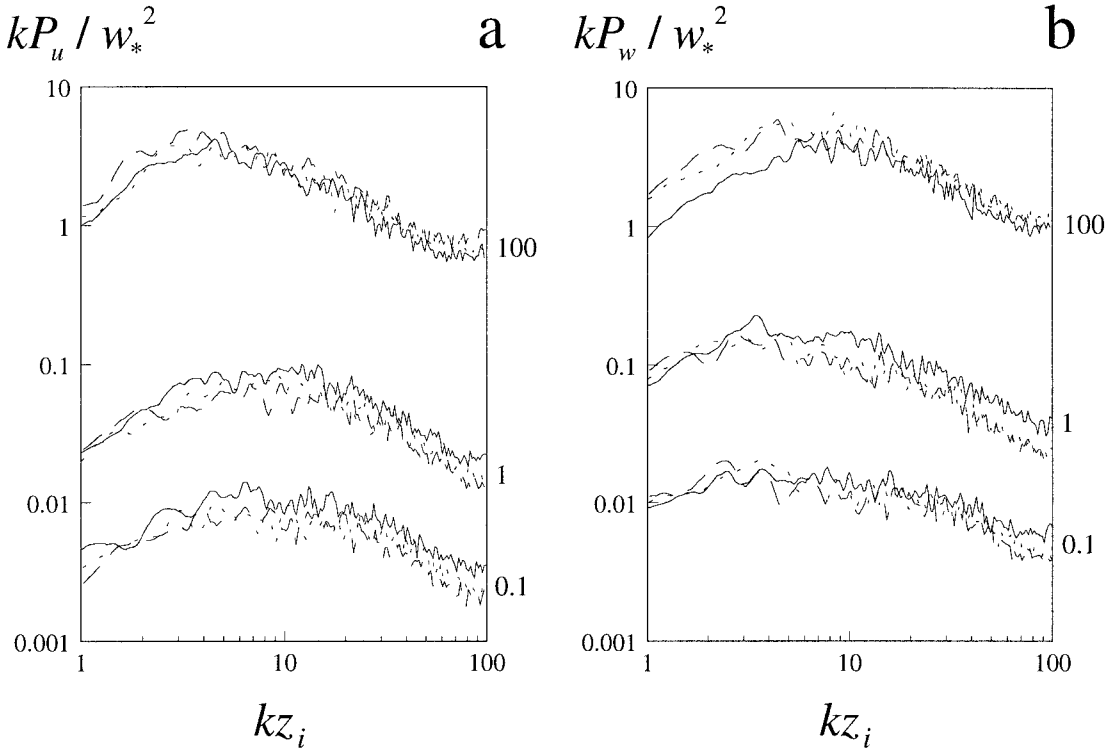

FIG. 2. Normalized horizontal (a) and vertical (b) velocity spectra in the simulated CBL at different fetches along the test section: $x = 3.98$ m, solid lines; $x = 5.63$ m, dashed lines; and $x = 7.28$ m, dotted lines. Figures at the right edges of the plots are multipliers for spectra measured at different heights: 0.1 for $z/z_i = 0.2$, 1 for $z/z_i = 0.6$, and 100 for $z/z_i = 1$.

the u spectra measured at $z/z_i = 0.2$ and $z/z_i = 0.6$. Such behavior of the velocity spectra in the near-wall region is well in accordance with the theoretical analysis by Tschen (1953) and Gisina (1966), who predicted a -1 spectral power dependency on k in regions where the turbulence is affected by the mean-flow shear.

In the entrainment layer ($z/z_i = 1$), the w spectrum measured at $x = 3.98$ m displays a markedly smaller energy level for large-scale fluctuations than the spectra from subsequent locations (Fig. 2b). A reason for this could be a stronger damping effect of the capping inversion at smaller fetches, where the initially imposed temperature increment is not yet diluted, see Fig. 3 in FKRP. The stronger damping results in a reduction of the number and size of buoyant thermals overshooting the inversion. The smaller-scale vertical motions are less affected by this damping. In the u spectra at the same height (the upper group of curves Fig. 2a), the damping effect of the capping inversion on larger-scale motions is not observed. The suppressive influence of stable stratification on the horizontal velocity fluctuations is probably compensated here by sideward motions resulting from the destruction of thermals in the entrainment zone.

We continue the measured spectra evaluation with consideration of the P_w/P_u spectral ratio within different wavenumber ranges. This characteristic is essential for making assumptions concerning the local isotropy of turbulence and the existence of inertial subranges in the measured spectra. Both aspects are of practical importance when the TKE dissipation rate and the destruction rate of the temperature fluctuations are evaluated using the measured spectra.

Local isotropy was introduced by Kolmogorov (1941) as homogeneity plus isotropy of the small scales of turbulent motions (Mestayer 1982). Another concept put forward by Kolmogorov was that of the inertial subrange, the energy cascade interval in the turbulence spectrum where no energy enters the system from the outside and no energy dissipates (Panofsky and Dutton 1984). In the inertial subrange, the energy spectrum is isotropic and does not depend on viscosity. The spectrum shape is thus determined only by the energy flux over the spectrum. This flux is equal to the energy dissipation rate ε. It follows from the dimensional analysis by Kolmogorov (1941) that in the inertial subrange

$$P_i(k) \sim \varepsilon^{2/3} k^{-5/3}, \tag{2}$$

where $P_i(k)$ is the spectral density of the velocity component u_i. Obukhov (1949) has shown that the assumptions of the Kolmogorov theory lead also to a $-5/3$ law in the inertial subrange spectrum of temperature fluctuations.

Local isotropy of turbulence and the presence of the inertial subrange in spectra are conditioned by a sufficiently high turbulent Reynolds number of the flow, Re_l

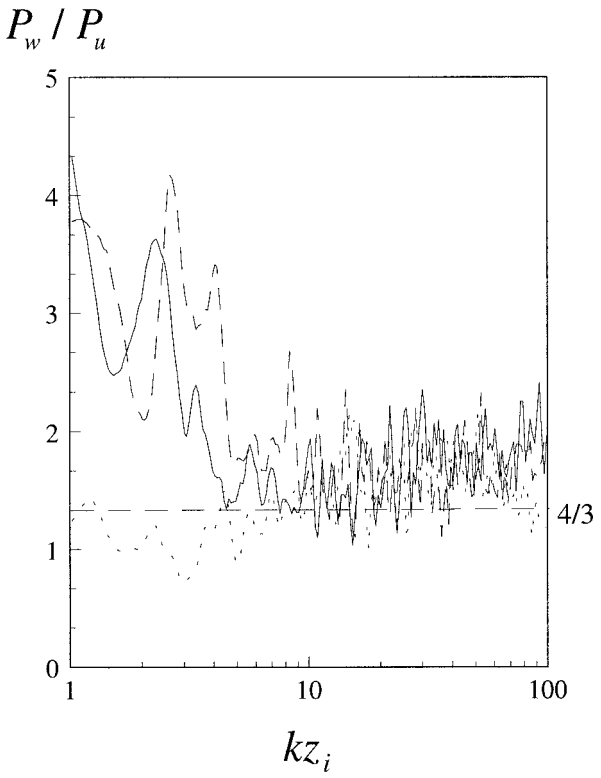

FIG. 3. Spectral ratio P_w/P_u at the 5.63-m fetch as a function of the dimensionless wavenumber at different dimensionless elevations in the simulated CBL: $z/z_i = 0.2$ (solid line), $z/z_i = 0.6$ (dashed line), and $z/z_i = 1$ (dotted line).

$= \boldsymbol{ul}/\nu$, where $\boldsymbol{u}$ is the representative turbulence velocity scale, $\boldsymbol{l}$ is the integral turbulence length scale, and ν is the kinematic air viscosity. According to the analysis of Tennekes and Lumley (1982), Re_l has to be of the order 10^3 or more to justify the employment of the Kolmogorov theory relationships for spectra in the inertial subrange. In the wind tunnel experiments considered, $\boldsymbol{u}$ is of the order 0.1 m s^{-1}, and $\boldsymbol{l}$ is about 0.5 m (FKRP), which gives $\mathrm{Re}_l \approx 3 \times 10^3$ (with $\nu = 1.5 \times 10^{-5}$ m^2 s^{-1}), thus providing grounds for expecting local isotropy features of turbulence in larger-wavenumber spectral ranges. Characteristic value of the Reynolds number $\mathrm{Re}_\lambda = \boldsymbol{u}\lambda/\nu$ based on the Taylor microscale λ in the wind tunnel CBL is about 50 (with $\lambda = 10^{-2}$ m). The estimate of λ results from $\lambda^2 = 15\nu\boldsymbol{u}^2/\varepsilon$, where ε is taken equal 10^{-2} m^2 s^{-3} (see the dissipation rate data in section 4).

Under conditions of local isotropy, the Kolmogorov theory predicts the P_w/P_u ratio in the inertial subrange to be equal to 4/3. The velocity spectra from the wind tunnel are checked against this criterion in Fig. 3. In the main portion of the CBL, the log-spectra of both velocity components (see Figs. 1 and 2) have linear parts at $kz_i > 10$, which may be evidence of the inertial spectral regime. With these wavenumbers, the values of P_w/P_u for all altitudes given in Fig. 3 are between 1.3 and 2, and therefore slightly exceed the local-isotropy prediction. There may be a physical reason for this excess, for example, the insufficiency of the pressure fluctuations to isotropize turbulence in the presence of dominating buoyant forcing, which favors vertical motions. This explanation is presented in Schmidt and Schumann (1989), who have found even stronger departure from local isotropy in their LES velocity spectra. Nevertheless, the proximity of the turbulence regime in the wind tunnel CBL to the conditions of local isotropy may be inferred from Fig. 3 for the wavenumber range $10 < kz_i < 80$.

For small and moderate wavenumbers ($kz_i < 10$), the behavior of P_w/P_u differs in the CBL mixed core and in the entrainment zone. In the mixed layer region (two lower dimensionless elevations in Fig. 3), the P_w/P_u ratio displays an overall tendency to decrease with an increasing wavenumber. The shapes of the two corresponding curves closely resemble each other within the range of kz_i from 1 to 6, but the P_w/P_u function at $z/z_i = 0.6$ is shifted to larger wavenumbers compared to P_w/P_u at $z/z_i = 0.2$. Such a translation of scale dependence from lower to higher levels inside the mixed layer is quite a remarkable feature of the obtained spectral ratio. From a physical point of view, this means that the distribution of energy between the vertical and horizontal velocity fluctuations at smaller wavenumbers contains a hidden length scale, which is apparently related to the distance from the wall. This may be a manifestation of the self-similarity of the large-scale turbulent structures in the CBL mixed core.

The dependence of P_w/P_u on k at small wavenumbers within the entrainment zone supports our earlier findings concerning the vertical motion suppression at the CBL top and the enhancement of the horizontal velocity fluctuations by the sideward spreading of air from rising thermals.

One more important characteristic of the CBL turbulence regime is the wavelength λ_{wm} corresponding to the maximum in the vertical velocity spectrum kP_w. Values of λ_{wm} from the wind tunnel CBL model are given in Fig. 4 together with data from other sources.

Close to the CBL top our measurements do not predict a drastic decay of λ_{wm} as observed in the data from the atmospheric study by Caughey and Palmer (1979). The small values of λ_{wm} in their case could be the effect of a very strong capping inversion. However, in the vicinity of $z/z_i = 1$ the wind tunnel data are reasonably close to the atmospheric data of Graf and Schumann (1992), who in addition used a LES model to reproduce the atmospheric situation. The wavelengths of spectral maxima from the wind tunnel model increase above the entrainment zone. Similar behavior of λ_{wm} was observed and modeled by Graf and Schumann (1992). The increase of λ_{wm} in the atmosphere can be associated with waves generated above the inversion under the condition of a sufficiently strong stable stratification (large Ri_N). In the wind tunnel model, Ri_N is comparatively small, and the λ_{wm} growth above the entrainment region results from

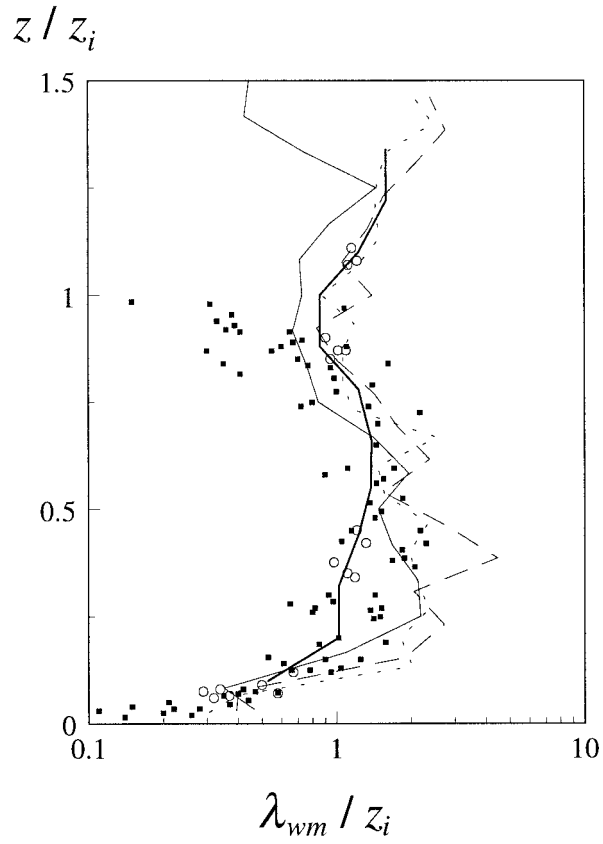

FIG. 4. Changes with the height of the wavelength corresponding to the maximum in the vertical velocity spectrum. Data from the wind tunnel model at $x = 3.98$ m, $x = 5.63$ m, and $x = 7.28$ m are shown by solid, dashed, and dotted lines, respectively. Points are atmospheric measurements of (squares) Caughey and Palmer (1979) and (circles) Graf and Schumann (1992). The heavy solid line represents the LES model data from Graf and Schumann (1992).

the increase of the separation distances between the narrow updrafts, overshooting into the turbulence-free zone.

In the lower part of the CBL, where λ_{wm} rapidly increases with height, all data sources represented in Fig. 4 provide close results. There is a noticeable scatter of the wind tunnel data from the mixed core of the CBL. The main reason for the scatter is the ambiguity of defining the spectrum maximum due to the flatness of spectral curves in this flow region, see discussion to Fig. 2. In this situation, the *w* spectrum often has two or more peaks approximately of the same magnitude within an extended range of *k*.

A comparison of the wind tunnel velocity spectra with spectral data from the water tank study of Deardorff and Willis (1985), and from the LES study by Schmidt and Schumann (1989) is presented in Fig. 5. In both studies, the shear-free atmospheric CBL was modeled. The CBL turbulence statistics from these studies were compared with their wind tunnel counterparts in FKRP, where larger values of the *u*- and *w*-velocity component variances were discovered in the sheared wind tunnel CBL. These larger values are clearly seen in the *u* and *w* spectra corresponding to the two lower measurement locations in Figs. 5a and 5b. At smaller wavenumbers ($kz_i < 8$), the wind tunnel *u* spectra (Fig. 5a) are smaller than the water tank ones and only slightly exceed the LES spectral values. The water tank data in this scale range presumably exhibit the effect of horizontal inhomogeneity of the surface heat flux, which was first pointed out by Schmidt and Schumann (1989) [see also discussion in Fedorovich and Mironov (1995) and in FKRP]. Larger *w*-spectral values from the wind tunnel model in the low-wavenumber interval may be explained by the contribution of quasi-steady cellular circulations to the velocity variance in the wind tunnel CBL. This contribution was discussed in FKRP. Near the CBL top, at $z/z_i = 1$, where the turbulence regime is practically unaffected by the surface shear, the wind tunnel spectra are close to the spectral curves from the other model studies.

With an increasing wavenumber, the LES spectra decrease while the wind tunnel spectral curves enter their characteristic flat parts. As a result, with kz_i larger than 10, the wind tunnel spectra of both velocity components are larger than their water tank and LES counterparts. At all altitudes represented in Fig. 5, the normalized velocity spectra from the wind tunnel model display linear parts, which can be fairly approximated by the $-5/3$ (for the normalized spectra by $-2/3$) power laws of the Kolmogorov (1941) inertial-subrange theory. These linear parts, although clearly seen in the plots, are rather short.

The estimation of the Kolmogorov turbulence microscale $\eta = (\nu^3/\varepsilon)^{1/4}$ in the tunnel flow yields $\eta = 10^{-3}$ m. At the same time, the observed linear subranges in the wind tunnel spectra are within $30\ \text{m}^{-1} < k < 250\ \text{m}^{-1}$, which corresponds to $3 \times 10^{-2} < k\eta < 2.5 \times 10^{-1}$. The upper limit in the last expression is of the order of $k\eta$ magnitude found by Champagne (1978) to be critical for existence of the inertial subrange. Considering the above estimate together with previously obtained estimates for Re_l and Re_λ, taking into account the measured P_w/P_u ratio and shortness of the $-5/3$ intervals in spectra, we admit that the reproduced turbulence regime is just at the border of what is required for existence of the inertial subrange in the turbulence spectra.

The turbulence timescales in the wind tunnel CBL may be evaluated in the following way.
The characteristic turbulence timescale:

$$t_l = \frac{\boldsymbol{l}}{\boldsymbol{u}} = \frac{0.4\ \text{m}}{0.1\ \text{m s}^{-1}} = 4\ \text{s}.$$

Timescale corresponding to the Taylor microscale:

$$t_\lambda = \frac{\lambda}{\boldsymbol{u}} = \frac{0.01\ \text{m}}{0.1\ \text{m s}^{-1}} = 0.1\ \text{s}.$$

Kolmogorov timescale:

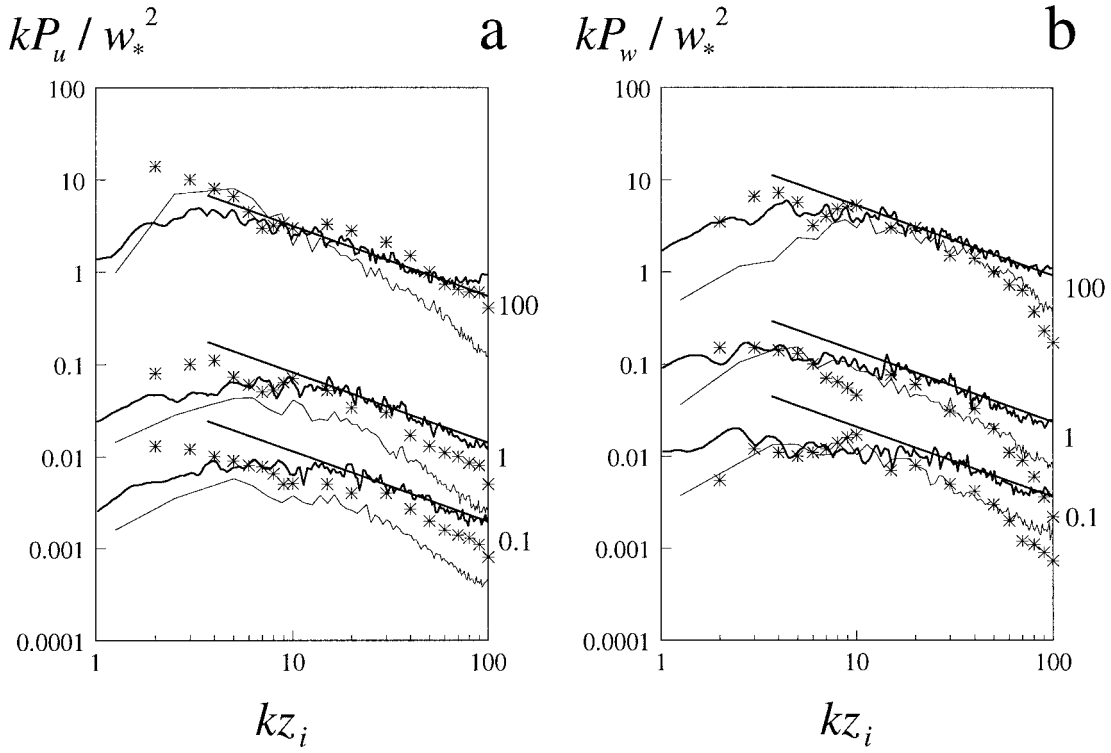

FIG. 5. Normalized horizontal (a) and vertical (b) velocity spectra in the simulated CBL at $x = 5.63$ m (heavy lines) compared with water tank results of Deardorff and Willis (1985) (points) and LES data of Schmidt and Schumann (1989) (lines). Heights and corresponding multipliers are the same as in Fig. 2. Straight lines represent $-5/3$ spectral law in the inertial subrange.

$$\tau_\eta = \left(\frac{\nu}{\varepsilon}\right)^{1/2} = \left(\frac{1.5 \times 10^{-5}}{10^{-2}}\right)^{1/2} = 0.04 \text{ s}.$$

Convective timescale:

$$\tau_* = \frac{z_i}{w_*} = \frac{0.3 \text{ m}}{0.2 \text{ m s}^{-1}} = 1.5 \text{ s}.$$

In the wind tunnel CBL, the mean-flow deformation is about 0.1 m s^{-1} over 5 m. Therefore, the timescale of the mean-flow evolution (50 s) is much larger than any of the turbulence scales in the CBL. This leads to the assumption that turbulent fluctuations are in the quasi-equilibrium with the mean flow, and therefore the flow may be considered homogeneous with respect to its turbulence regime.

In the spectra from LES models, as pointed out by Deardorff (1971) and Schmidt and Schumann (1989), the high-wavenumber ranges are deformed due to the artificial smoothing on the shortest resolved scales and due to the inability of LES models to resolve a significant portion of the larger-scale end of the inertial subrange. Both of these effects are responsible for the comparatively fast decay and the excessive curvature of the spectra from the LES at large wavenumbers.

Published velocity spectra from the atmospheric CBL are often not sufficiently documented to use them for verification of the wind tunnel data. Many of these spectra are either plotted in schematic or generalized form like those from Kaimal et al. (1976), presented in dimensionless form using special scales like spectra from Mann et al. (1995), grouped within height ranges as in Young (1987), or given in initial form without a clear indication of the integral parameters of the convective regime studied (Caughey and Palmer 1979). The above circumstances greatly hamper a direct comparison between the wind tunnel velocity spectra and the atmospheric CBL spectral data.

In order to transform the atmospheric spectra of Caughey and Palmer (1979) and the wind tunnel spectral measurements into a common domain we have used a kind of internal spectral normalization. It implies the normalization of the energy spectrum nP_i by its maximum value in the production range, $(nP_i)_m$, and the normalization of the frequency by the value n_m at which this maximum is achieved. Resulting dimensionless spectra are not suited for making quantitative conclusions, but can be useful for evaluating the similarity of the spectral shape. In Fig. 6, the wind tunnel velocity component spectra are plotted together with the atmospheric spectra measured at $z/z_i = 0.9$, which is in the lower portion of the entrainment zone. The shapes of the modeled and measured spectra at this elevation are similar in the vicinity of the spectral maxima, where

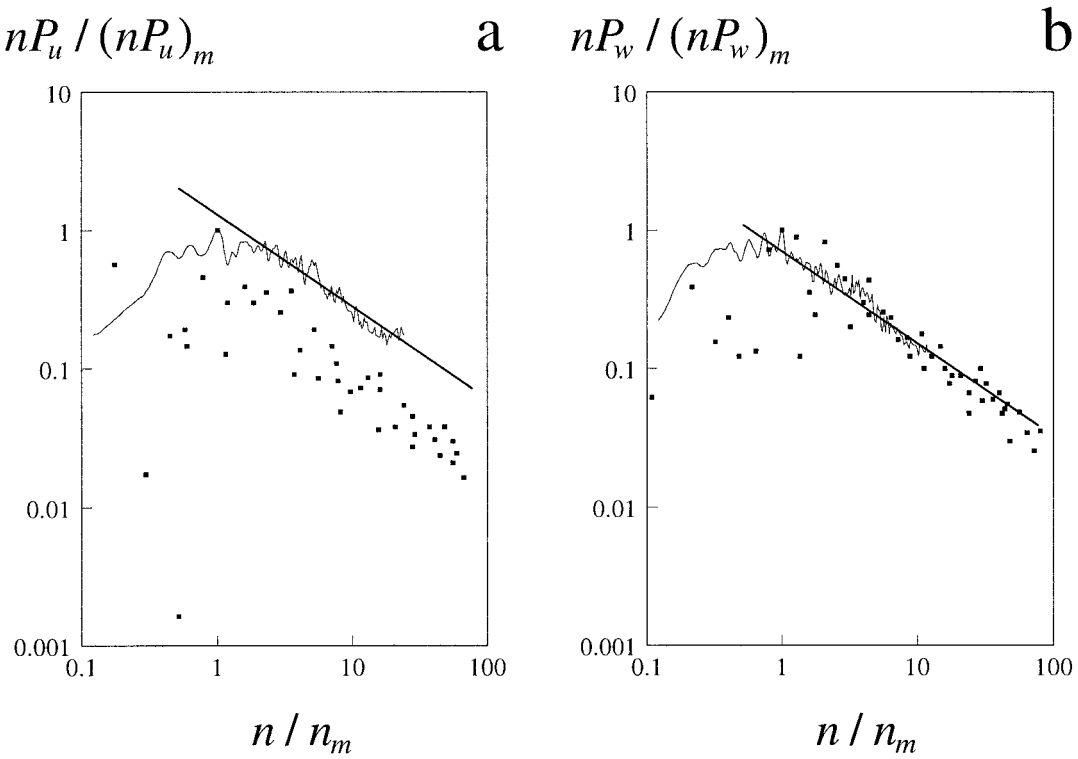

FIG. 6. Normalized horizontal (a) and vertical (b) velocity spectra in the simulated CBL at $x = 5.63$ m (lines) compared with the atmospheric CBL data of Caughey and Palmer (1979) (points) for $z/z_i = 0.9$. Straight lines correspond to $-5/3$ law.

several distinctive peaks are resolved in the wind tunnel spectra. The atmospheric data follow the inertial-subrange power law within longer frequency bands than the wind tunnel spectra. The comparison presented gives a general idea of the proportion between extensions of the inertial subranges in the atmospheric and in the wind tunnel CBL velocity spectra. The inertial subranges of the atmospheric spectra are typically an order of magnitude longer.

b. Temperature spectra

The temperature spectra from the wind tunnel model are grouped in Fig. 7. At the two lower elevations in the simulated CBL the T spectra are similar to the u spectra (Fig. 2a). They are relatively flat in the production region and bear evidence of a vast range of the temperature fluctuation scales, which almost equally contribute to the spectral energy, see Fig. 7a. The longitudinal variability of the T spectra in the CBL lower portion is small compared with the velocity spectra, and the normalized temperature spectra at all fetches almost coincide. In the entrainment zone, at $z/z_i = 1$, the temperature spectra have pronounced maxima at a kz_i of about 3, and their decay in the high-wavenumber range is faster than that of the T spectra measured at lower levels. From the spectra at $z/z_i = 1$ the effect of inversion strength on the temperature fluctuation magnitude is clearly seen. Larger temperature variance, and thus larger T spectra values, are observed at $x = 3.98$ m, where the comparatively large temperature increment across the entrainment zone enhances temperature fluctuations (see temperature variances at the inversion in Fig. 6a of FKRP). This enhancement is rather uniformly distributed over the entire spectral range.

A smaller inversion strength in the wind tunnel experiments is the reason for the lower position of the corresponding spectrum curve in Fig. 7b as compared with temperature spectra from the water tank and LES studies. In the bulk of the CBL, the wind tunnel spectra are located close to the LES spectra, but are not as protuberant as the latter ones. It is not clear to us what the source of the exaggeration of the small-scale temperature fluctuations in the water tank simulations of Deardorff and Willis (1985) could be.

The comparison of Fig. 7b and Fig. 5 shows that the $-5/3$ linear intervals in the temperature log-spectra from the wind tunnel model are even shorter that in the velocity spectra. However, we still consider them to be sufficiently pronounced in order to use the assumptions of the inertial-subrange theory for the evaluation of the temperature destruction rates from the measured spectra. In Fig. 7c, the wind tunnel and atmospheric spectra are plotted together using the same scaling as applied to the velocity spectra in Fig. 6. It is easy to notice that the

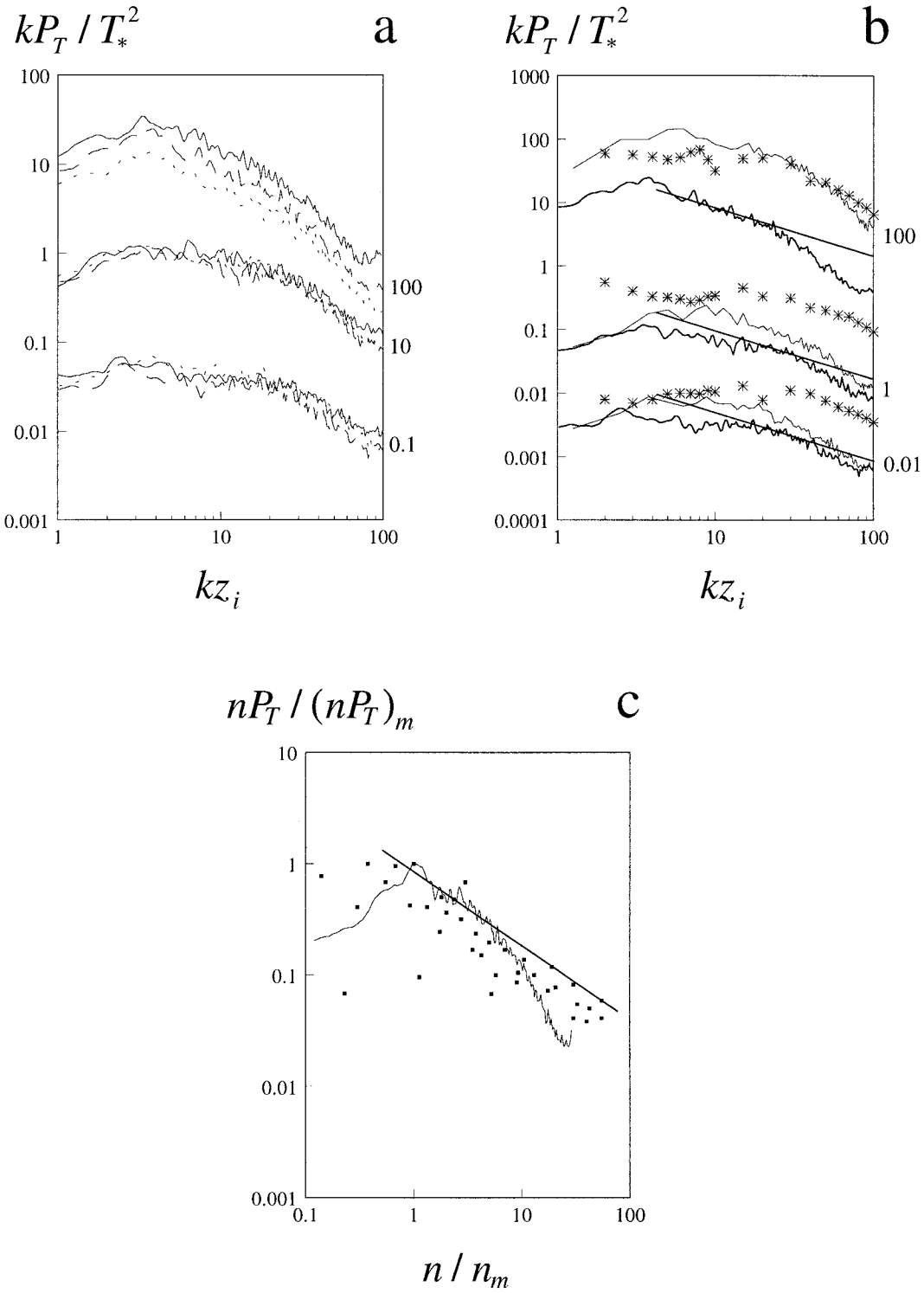

FIG. 7. Temperature spectra in the simulated CBL: (a) at different distances from the test section inlet (notation corresponds to Fig. 2); (b) compared with the water tank and LES data (notation as in Fig. 5, but the multiplier for spectra at z/z_i = 0.2 is 0.01 instead of 0.1); (c) compared with the atmospheric CBL data (notation corresponds to Fig. 6).

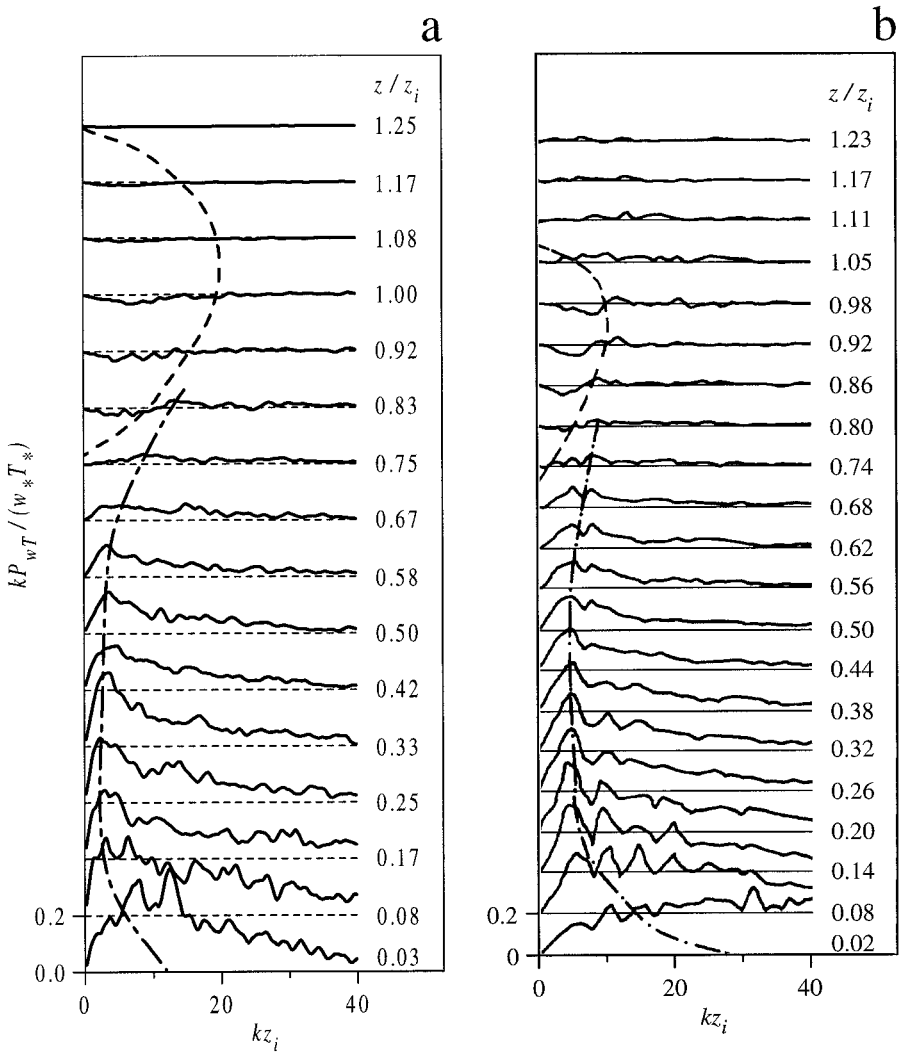

FIG. 8. Heat flux cospectra from the wind tunnel model of the CBL: (a) compared with the LES results of Schmidt and Schumann (1989); (b) spectra scales are shown at the left edges of the plots. Dashed and dotted lines indicate vertical changes of spectra maxima positions in the mixed layer; dashed lines envelope regions of negative wT correlation within the entrainment zone.

$-5/3$ law part in the atmospheric spectrum extends much farther than in the wind tunnel spectrum.

c. Heat flux spectra

In this section we consider spectra of the vertical turbulent kinematic heat flux $\overline{w'T'}$ (also called the temperature flux), which are actually cospectra of the vertical velocity and temperature fluctuations. In Fig. 8, the heat flux spectra from the wind tunnel model are plotted in the same form as the LES spectra of Schmidt and Schumann (1989) in order to facilitate their comparison. It is clear from the plot that in the wind tunnel CBL heat is transported upward by comparatively large-scale turbulent structures. The shape of the wind tunnel cospectrum at $z/z_i = 0.03$ is very similar to that of the heat flux spectrum measured by Kaimal et al. (1976) in the atmospheric CBL at $z/z_i = 0.04$, while the LES spectrum corresponding to $z/z_i = 0.02$ more resembles the atmospheric heat flux spectrum from Kaimal et al. (1976) at a much smaller height, $z/z_i = 0.003$. The influence of the surface shear in the wind tunnel CBL can be one reason for a comparatively weak correlation between w and T fluctuations at larger wavenumbers. We have already noted that the shear influence apparently shifts the w spectra to higher frequencies. Velocity fluctuations induced by shear are not coupled with temperature disturbances, rather merely stochastically mixed with them. Near the surface (at $z/z_i = 0.03$), this results in the comparatively fast decay of the wind tunnel cospectrum with increasing wavenumber.

In the lower quarter of the CBL, the wind tunnel spectra consistently display two peaks at small wavenumbers. These peaks may be related to narrow warm

updrafts (positive w' correlate with positive T') and to wide cold downdrafts (negative w' correlate with negative T'). With increasing height, these peaks merge into one comparatively broad maximum located close to $kz_i = 5$. The LES spectra in the main portion of the CBL have their maxima approximately at the same wavenumber. These locations of the cospectra maxima are in accordance with the observation of Kaimal et al. (1976), who found that motions with scales of the order of z_i (which corresponds to $kz_i = 6.28$) are main contributors to the turbulent transport of heat in the atmospheric CBL.

The magnitude of the cospectrum decreases toward the upper part of the CBL, and the spectral maximum shifts to larger wavenumbers. In the lower portion of the entrainment region, at $z/z_i > 0.8$, negative spectral components appear at small wavenumbers. These components represent large-scale cold updrafts and warm downdrafts, responsible for the negative heat flux of entrainment. An association of the entrainment in the atmospheric CBL with larger-scale turbulent motions was revealed by the experimental studies of Kaimal et al. (1976), Wilczak and Businger (1983), and Mahrt and Paumier (1984). Higher-frequency components of the heat flux in the entrainment zone retain positive values and gradually decay toward the CBL top ($z/z_i = 1.2$). In the wind tunnel cospectra above this level we have not found ''small but significantly positive heat flux values,'' discovered by Schmidt and Schumann (1989) in their LES cospectra.

4. Dissipation rate of TKE and destruction rate of temperature fluctuations

For the evaluation of the TKE dissipation rate ε from the wind tunnel velocity spectra we employ the following relationships of the Kolmogorov inertial-subrange theory (Tennekes and Lumley 1982):

$$P_u(k) = \alpha\varepsilon^{2/3}k^{-5/3} \tag{3a}$$

$$P_w(k) = \frac{4}{3}\alpha\varepsilon^{2/3}k^{-5/3}, \tag{3b}$$

where the value of the dimensionless parameter α is taken equal 0.52 as recommended in Andreas (1987) and Schmidt and Schumann (1989). From a practical point of view, the procedure of the determination of ε consists of separating out the inertial subrange in a given log-spectrum using the $-5/3$ law criterion, and of consequent derivation of ε from (3a) or (3b) using the least-squares approximation of the inertial-subrange spectrum.

Our analysis in section 3 has shown that assumptions of the inertial-subrange theory, including the assumption of the local isotropy, are only approximately satisfied in the wind tunnel CBL. Thus we cannot expect horizontal and vertical velocity spectra to provide exactly the same values of ε. The applicability of Eqs. (3) to spectra obtained near the upper edge of the entrainment zone and in the outer flow, where spectral inertial subranges are very short, seems to be rather questionable.

This is the reason why ε profiles from the wind tunnel model shown in Fig. 9a are truncated at $z/z_i > 1.2$, although the velocity spectra have also been measured at much higher levels. In the main portion of the CBL, discrepancies between the values of the dissipation rate alternatively derived from the u spectra [using Eq. (3a)] and from the w spectra [using Eq. (3b)] are much smaller than the scatter of data from other sources represented in Fig. 9a. The smallest dissipation rate values in this plot are from the LES of Schmidt and Schumann (1989), who have modeled a pure shear-free CBL. Larger values of ε in the lower portion of the CBL from the water tank model of Deardorff and Willis (1985) are presumably a result of the TKE overproduction due to the aforementioned horizontal variations of the bottom heat flux in their experiments. The profiles of ε measured in nature (in the ocean and in the atmosphere) are in relative accordance with each other and are characterized by the enhancement of data scatter toward the CBL top. Apparently, this is the effect of nonbuoyant contributions to the TKE production in natural convective flows. Comparatively large ε values in the wind tunnel CBL result from the combined influence of shear, cellular circulations, and the weak damping effect of capping inversion. All these factors have been considered in previous sections of the paper and in FKRP. In the lower third of the CBL, the wind tunnel model gives higher ε values than any other data source. We believe this to be a result of the essential shear contribution in this region, as well as the disclosure of a certain insufficiency of the inertial-subrange assumptions in the near-surface region of the flow. This insufficiency also causes marked divergence of ε profiles, derived from Eq. (3a) and Eq. (3b), respectively, in the close vicinity of the surface.

The local integral budgets of TKE have been evaluated in order to quantify the ratio between the TKE production and dissipation in the CBL model (see also the TKE budget considerations in FKRP). In terms of $(I_{\text{prod}} - I_{\text{diss}})/I_{\text{prod}}$, the budget discrepancy turned out to be of the order 0.1.

The destruction rate of the temperature fluctuations, ε_T (we define it here as destruction of the temperature half-variance), is obtained from the inertial-subrange temperature spectra using the Obukhov (1949) law expressed by

$$P_T(k) = \beta\varepsilon_T\varepsilon^{-1/3}k^{-5/3}, \tag{4}$$

where $\beta = 0.8$ is a dimensionless coefficient (Andreas 1987; Schmidt and Schumann 1989). The procedure for the derivation of ε_T from the T spectra is analogous to the evaluation of ε from the velocity spectra, but in this case we have the choice of substituting ε in Eq. (10) determined either from Eq. (3a) or from Eq. (3b). It is

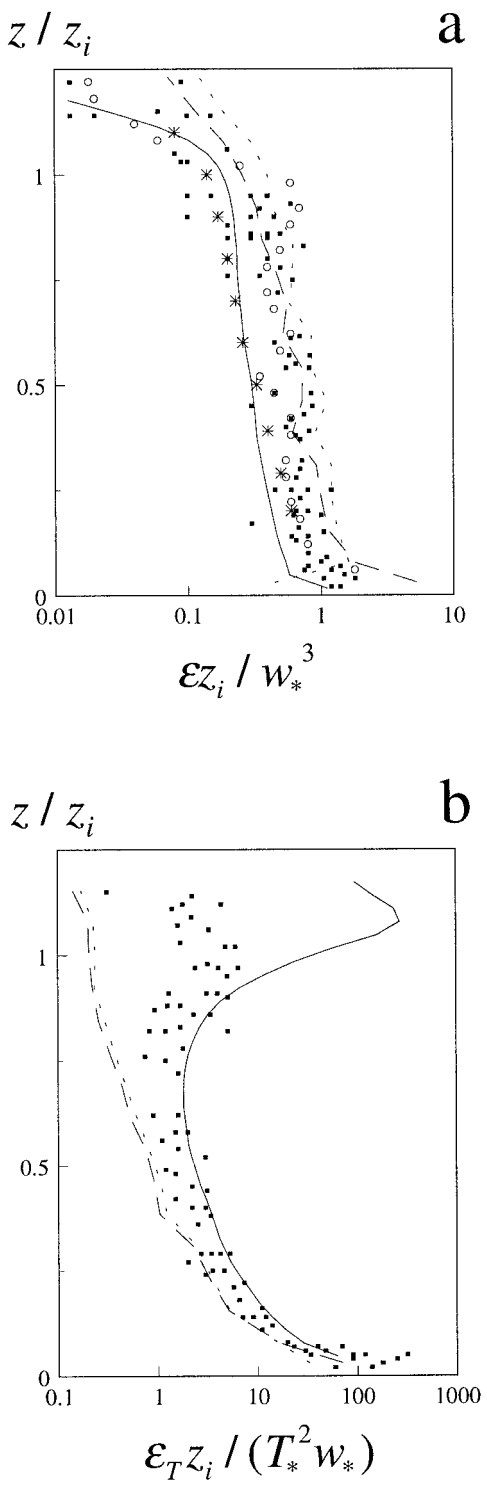

FIG. 9. Normalized profiles of the TKE dissipation rate (a) and the temperature fluctuations destruction rate (b). Dashed lines and dotted lines show ε values derived from the wind tunnel u spectrum and w spectrum respectively. Solid squares are atmospheric data from Caughey and Palmer (1979). Solid curves show results from the LES model of Schmidt and Schumann (1989) (courtesy of U. Schumann). In (a), asterisks are water tank data of Deardorff and Willis (1985) and circles are oceanic data of Shay and Gregg (1986).

seen, however, from Fig. 9b that the difference between the resulting ε_T profiles is small. This is not surprising because the dependence of $P_T(k)$ on ε in Eq. (4) is rather weak. In the lower half of the layer, where the Deardorff (1970) scaling works appropriately, the discrepancies between ε_T from the three datasets represented in Fig. 9b are not very large. At the CBL upper interface, where the turbulence regime is essentially governed by the damping effect of capping inversion, the ε_T profiles from the wind tunnel, atmospheric, and LES studies drastically diverge. The wind tunnel model with typically moderate $\mathrm{Ri}_{\Delta T}$ gives the smallest values of ε_T. Both atmospheric and LES datasets reveal maxima in the ε_T profiles in the vicinity of $z/z_i = 1$. These maxima are products of exaggerated temperature fluctuations in the entrainment layer with a strong stable temperature gradient (large $\mathrm{Ri}_{\Delta T}$). The budget evaluation for the temperature variance performed in the same way as for the TKE has revealed budget discrepancies of about 0.5.

5. Conclusions

The results of the wind tunnel velocity and temperature spectral measurements reported in the present paper verify the capability of the thermally stratified wind tunnel of the IHW to reproduce the main features of turbulence spectral dynamics in the atmospheric CBL. A point of particular interest in this study has been the identification of wind shear effects, which are usually omitted in traditional laboratory CBL models.

In the bulk of the simulated CBL, the buoyancy was found to be the dominant factor of turbulence production at smaller wavenumbers, while the shear contribution was apparently increasing with the wavenumber growth. The combined effect of buoyant and shear forcings in the simulated CBL could be a reason for the elongation and flatness of the production ranges of the spectra measured.

The model velocity spectra have been checked against the 4/3 isotropic criterion for the vertical to horizontal spectral ratio. With $kz_i \geq 10$, this ratio was found to be in the range from 1.3 to 2, which is slightly higher than the local-isotropy value. With smaller wavenumbers, the spectral ratio behaved differently in the mixed core of the CBL and in the entrainment zone. A translation of scale dependence from lower to higher levels has been discovered in the low-frequency spectra, a property that apparently points to the self-similarity of large-scale turbulence structures in the CBL.

Wind tunnel data on the wavelength, corresponding to the maximum in the vertical velocity spectrum, were found to be noticeably scattered. The main reason for this was the ambiguity in defining the spectrum maximum when motions of a variety of scales equally contribute to the turbulence production. Under such conditions, one wavelength does not seem to be a representative parameter for characterizing the CBL turbulence regime.

The comparison of the wind tunnel velocity spectra with water tank and LES data for the shear-free CBL enabled identification of the wavenumber dependence of the shear contribution to the turbulence production. At small wavenumbers ($kz_i < 8$), where larger-scale buoyant structures were dominant, the wind tunnel spectral values were close to those obtained in the shear-free CBL. At larger wavenumbers, the wind tunnel spectra contained more energy than the relatively rapidly decaying spectra from water tank and LES studies of shear-free convection.

Temperature spectra in the wind tunnel model gave evidence for a vast range of the temperature fluctuation scales contributing almost equally to the temperature variance in the production range. The influence of the near-surface shear was pointed out as a possible reason for the comparatively weak correlation between w and T fluctuations at larger wavenumbers in the lower portion of the wind tunnel CBL.

In the mixed core and in the entrainment zone of the simulated CBL, log-spectra of velocity and temperature featured apparent linear $-5/3$ law subranges at $kz_i > 10$. Nevertheless, typical extensions of these subranges in the wind tunnel CBL were quite short, up to one order of the kz_i magnitude. Based on the vertical to horizontal velocity spectral ratio and on the estimate of the characteristic turbulent Reynolds number of the flow ($\mathrm{Re} \approx 3 \times 10^3$), the inertial-subrange theory assumptions were used for the evaluation of the turbulence dissipation rates from the velocity spectra.

The turbulence kinetic energy dissipation rate proved to be comparatively large over the whole depth of the wind tunnel CBL. This resulted from the combined influence of shear, local cellular circulations, and the weak capping inversion damping. At the same time, the values of the temperature fluctuation destruction rate in the wind tunnel model turned out to be quite small, especially in the upper portion of the simulated CBL, where no essential sources of temperature fluctuation production have been identified.

Acknowledgments. The reported study has been carried out within the research project ''Windkanaluntersuchung der Turbulenzdynamik, Transportprozesse und Ausbreitungsvorgänge in konvektiven Grenzschichten mit angehobener Temperaturinversion,'' funded by the German Science Foundation (DFG). The authors are thankful to Erich Plate, the director of the IHW, for his supervision of the study, and to Ulrich Schumann for providing the LES spectral data. The second author gratefully acknowledges support from the Alexander von Humboldt Foundation Germany, and from the Department of Physics, University of Genoa, Italy.

APPENDIX

Details of Spectra Calculation

Fourier transform of a finite time series with discrete sampling $\varphi(n\Delta t)$ is a discrete function of $m\Delta f$, where f is frequency (Hesselmann 1987):

$$\Phi(m\Delta f) = \Delta t \sum_{n=0}^{N-1} \varphi(n\Delta t) \exp[-2\pi i (m\Delta f)(n\Delta t)] = \Delta t \sum_{n=0}^{N-1} \varphi(n\Delta t) \exp(-2\pi i mn/N). \quad \text{(A1)}$$

The resolution in the frequency domain of a Fourier transform, derived from a finite time series with length T, is

$$\Delta f = \frac{1}{T} = \frac{1}{N\Delta t}. \quad \text{(A2)}$$

For collection of n_k records representing stationary (ergodic) random data, $\varphi_k(n\Delta t)$; $(k-1)T \le t \le kT$; $k = 1, 2, \ldots, n_k$, the one-sided autospectral density function P_φ is estimated by

$$P_\varphi(m\Delta f) = \frac{2}{n_k T} \sum_{k=1}^{n_k} |\Phi_k(m\Delta f)|^2, \quad \text{(A3)}$$

where Φ_k is the discrete Fourier transform defined by Eq. (A1).

Similarly, for two collections of n_k paired records $\varphi_k(n\Delta t)$ and $\psi_k(n\Delta t)$; $(k-1)T \le t \le kT$; $k = 1, 2, \ldots, n_k$, the one-sided cross-spectral density function $P_{\varphi\psi}$ is estimated by

$$P_{\varphi\psi}(m\Delta f) = \frac{2}{n_k T} \sum_{k=1}^{n_k} \Phi_k^*(m\Delta f)\Psi_k(m\Delta f), \quad \text{(A4)}$$

where the asterisk denotes complex conjugation, and Ψ_k is the finite Fourier transform of $\psi_k(n\Delta t)$. Contrary to the autospectral density function P_φ, which is real, the cross-spectral density function is complex: $P_{\varphi\psi} = C_{\varphi\psi} - iQ_{\varphi\psi}$. Its real part $C_{\varphi\psi}$ is called the coincident spectral density function. In the scientific literature, the term ''spectrum'' usually stands for the one-sided autospectral density function, and ''cospectrum'' for the one-sided coincident spectral density function.

Expressions (A1), (A3), and (A4) were employed in the present study for calculation of the velocity and temperature spectra and cospectra from the wind tunnel measurements. For the purpose of spectral averaging, every original time series was separated into 16 records, each containing 1024 measurement values. This corresponds to $n_k = 16$, $N = 1024$, and $T = 10.24$ s in Eqs. (A1)–(A4). The calculated spectra were subdivided into 400 equal intervals with respect to the logarithm of frequency, and the average spectral density value within each interval was calculated. This was done merely to improve the layout of the spectra when plotted in logarithmic scales.

Since the Taylor hypothesis was found to be applicable for the flow in the simulated CBL (FKRP), it was used to transfer the spectra from the frequency domain to the wavenumber one. Provided the mean-flow horizontal velocity u at the location of the spectral measurements is known, the following relationship between

the wavenumber k, the wavelength λ, and the frequency f may be employed:

$$k = \frac{2\pi}{\lambda} = \frac{2\pi f}{u}.$$

The wavenumber spectrum $P_\varphi(k)$ and the frequency spectrum $P_\varphi(f)$ are related by

$$P_\varphi(k) = \frac{u}{2\pi} P_\varphi(f).$$

Experimental spectra are usually presented with logarithmic scales of frequency or wavenumber (Jensen and Busch 1982; Panofsky and Dutton 1984). If the ordinates are $fP_\varphi(f)$ or $kP_\varphi(k)$, then the area in a log-frequency or log-wavenumber interval represents the contribution of the fluctuations in this interval to the variance of φ. One more advantage of these ordinates is their independence on the units of frequency or wavenumber selected, because $fP_\varphi(f) = kP_\varphi(k)$. Most of spectra from the wind tunnel experiments are shown in such a logarithmic frequency/wavenumber form.

REFERENCES

Adrian, R. J., R. T. D. S. Ferreira, and T. Boberg, 1986: Turbulent thermal convection in wide horizontal fluid layers. *Experiments in Fluids*, Vol. 4, Springer-Verlag, 121–141.

Andreas, E. L, 1987: Spectral measurements in a disturbed boundary layer over snow. *J. Atmos. Sci.*, **44,** 1912–1939.

Bendat, J. S., and A. G. Piersol, 1986: *Random Data Analysis and Measurement Procedures.* John Wiley & Sons, 566 pp.

Caughey, S. J., and S. G. Palmer, 1979: Some aspects of turbulence structure through the depth of the convective boundary layer. *Quart. J. Roy. Meteor. Soc.,* **105,** 811–827.

Cenedese, A., and G. Querzoli, 1994: A laboratory model of turbulent convection in the atmospheric boundary layer. *Atmos. Environ.*, **28,** 1901–1914.

Champagne, F. H., 1978: The fine-scale structure of the turbulent velocity field. *J. Fluid. Mech.,* **86,** 67–108.

Cooley, J. W., and J. W. Tukey, 1965: An algorithm for the machine calculation of complex Fourier series. *Math. Comput.,* **19,** 297–301.

Deardorff, J. W., 1970: Convective velocity and temperature scales for the unstable planetary boundary layer and for Raleigh convection. *J. Atmos. Sci.,* **27,** 1211–1213.

——, 1971: On the magnitude of the subgrid scale eddy coefficient. *J. Comput. Phys.,* **7,** 120–133.

——, and G. E. Willis, 1985: Further results from a laboratory model of the convective planetary boundary layer. *Bound.-Layer Meteor.,* **32,** 205–236.

Fedorovich, E., and D. V. Mironov, 1995: A model for shear-free convective boundary layer with parameterized capping inversion structure. *J. Atmos. Sci.,* **52,** 83–95.

——, R. Kaiser, M. Rau, and E. Plate, 1996: Wind-tunnel study of turbulent flow structure in the convective boundary layer capped by a temperature inversion. *J. Atmos. Sci.,* **53,** 1273–1289.

Gisina, F. A., 1966: The effect of mean velocity and temperature gradients on the spectral characteristics of turbulence. *Izv. Acad. Sci. U.S.S.R., Atmos. Oceanic Phys.*, **2,** 804–813 (English translation 487–491).

Graf, J., and U. Schumann, 1992: Simulation of the convective boundary layer in comparison to aircraft measurements. *Air Pollution Modeling and its Application,* Vol. IX, H. van Dop and G. Callos, Eds., Plenum Press, 587–593.

Grossman, R. L., 1982: An analysis of vertical velocity spectra obtained in the BOMEX fair-weather, trade-wind boundary layer. *Bound.-Layer Meteor.*, **23,** 323–357.

Hesselmann, N., 1987: *Digitale Signalverarbeitung.* Vogel Buchverlag, 216 pp.

Jensen, N. O., and N. E. Busch, 1982: Atmospheric turbulence. *Engineering Meteorology,* E. J. Plate, Ed., Elsevier, 179–231.

Kaimal, J. C., J. C. Wyngaard, D. A. Haugen, O. R. Coté, Y. Izumi, S. J. Caughey, and C. J. Readings, 1976: Turbulence structure in a convective boundary layer. *J. Atmos. Sci.*, **33,** 2152–2169.

Kolmogorov, A. N., 1941: Local structure of turbulence in the incompressible fluid at very high Reynolds numbers. *Dokl. Akad. Nauk S.S.S.R.,* **30,** 299–303.

Kumar, R., and R. J. Adrian, 1986: Higher order moments in the entrainment zone of turbulent penetrative thermal convection. *J. Heat Trans.,* **108,** 323–329.

Mahrt, L., and J. Paumier, 1984: Heat transport in the atmospheric boundary layer. *J. Atmos. Sci.*, **41,** 3061–3075.

Mann, J., K. J. Davis, D. H. Lenschow, S. P. Oncley, C. Kiemle, G. Ehert, A. Giez, and H. G. Schreiber, 1995: Airborne observations of the boundary layer top, and associated gravity waves and boundary layer structure. *Proc. Ninth Symp. on Meteorological Observations and Instrumentation*, Charlotte, NC, Amer. Meteor. Soc., 113–116.

Mason, P. J., 1992: Large-eddy simulation of dispersion in convective boundary layers with shear. *Atmos. Environ.,* **26A,** 1561–1571.

Mestayer, P., 1982: Local isotropy and anisotropy in a high-Reynolds-number turbulent boundary layer. *J. Fluid. Mech.,* **125,** 475–503.

Moeng, C.-H., and P. P. Sullivan, 1994: A comparison of shear- and buoyancy-driven planetary boundary layer flows. *J. Atmos. Sci.*, **51,** 999–1022.

Nieuwstadt, F. T. M., P. J. Mason, C.-H. Moeng, and U. Schumann, 1993: Large-eddy simulation of the convective boundary layer: A comparison of four computer codes. *Turbulent Shear Flows 8,* F. Durst et al., Eds., Springer-Verlag, 343–367.

Obukhov, A. M., 1949: Structure of the temperature field in turbulent flows. *Izv. Akad. Nauk S.S.S.R., Ser. Geogr. i Geofiz.*, **13,** 58–69.

Panofsky, H. A., and J. A. Dutton, 1984: *Atmospheric Turbulence.* John Wiley & Sons, 397 pp.

Poreh, M., M. Rau, and E. Plate, 1991: Design considerations for wind tunnel simulations of diffusion within the convective boundary layer. *Atmos. Environ.,* **25A,** 1250–1257.

Rau, M., and E. Plate, 1995: Wind tunnel modelling of convective boundary layers. *Wind Climate in Cities,* J. Cermak et al., Eds., Kluwer, 431–456.

Schmidt, H., and U. Schumann, 1989: Coherent structure of the convective boundary layer derived from large-eddy simulations. *J. Fluid. Mech.*, **200,** 511–562.

Sorbjan, Z., 1991: Evaluation of local similarity functions in the convective boundary layer. *J. Appl. Meteor.*, **30,** 1565–1583.

Shay, T. J., and M. C. Gregg, 1986: Convectively driven turbulent mixing in the upper ocean. *J. Phys. Oceanogr.*, **16,** 1777–1798.

Sykes, R. I., and D. S. Henn, 1989: Large-eddy simulation of turbulent sheared convection. *J. Atmos. Sci.,* **46,** 1106–1118.

Tennekes, H., and J. L. Lumley, 1982: *A First Course in Turbulence.* The MIT Press, 300 pp.

Tschen, C. M., 1953: On the spectrum of energy in turbulent shear flow. *J. Res. NBS,* **50,** 51–62.

Wilczak, J. M., and J. A. Businger, 1983: Thermally indirect motions in the convective atmospheric boundary layer. *J. Atmos. Sci.*, **40,** 343–358.

Young, G. S., 1987: Mixed layer spectra from aircraft measurements. *J. Atmos. Sci.,* **44,** 1251–1256.